Surface composition and structure of divertor tiles following the JET tokamak operation with the ITER-like wall

A. Lagoyannis[1], P. Tsavalas[1], K. Mergia[1,*], G. Provatas[1], K. Triantou[1], E. Tsompopoulou[1], M. Rubel[2],
P. Petersson[2], A. Widdowson[3], S. Harissopulos[1], T.J. Mertzimekis[4], and the JET contributors[**]

EUROfusion Consortium, JET, Culham Science Centre, Abingdon, OX14 3DB, UK
[1] *Fusion Technology Group, National Centre for Scientific Research ''Demokritos'', 15310 Aghia Paraskevi, Athens, Greece*
[2]*Department of Fusion Plasma Physics, Royal Institute of Technology (KTH), 100 44 Stockholm, Sweden*
[3]*Culham Centre for Fusion Energy, OX14 3DB Abingdon, Oxfordshire, United Kingdom*
[4]*Department of Physics, University of Athens, Zografou Campus, 15784, Athens, Greece*
*** See the author list of “Overview of the JET results in support to ITER” by X. Litaudon et al. to be published in Nuclear Fusion Special issue: overview and summary reports from the 26th Fusion Energy Conference (Kyoto, Japan, 17-22 October 2016)*

Abstract

Samples extracted from several divertor tiles following the 2011-2012 operation of JET with the ITER-Like wall were analyzed using ion beam analysis methods, X-ray fluorescence spectroscopy, scanning electron microscopy with energy dispersive spectroscopy analysis and X-ray diffraction. The emphasis was on the determination of light species and on material mixing including compound formation on the bottom and the outer divertor tiles. Deposition of deuterium, beryllium, carbon, nitrogen, oxygen, iron, chromium, nickel and molybdenum has been detected on all studied tiles. The thickest deposition, of around 4 μm, was measured on the bottom of the outer divertor, whereas the other surfaces (inner bottom and vertical outer) the co-deposits were around 1 μm. X-ray diffraction measurements have revealed the formation of the compound W_2C on all specimens.

---

[*] Corresponding Author: K. Mergia, kmergia@ipta.demokritos.gr

1. Introduction

Erosion, deposition and materials migration in fusion plasma devices, as well as fuel retention in plasma-facing components, are issues of great importance for the safe operation of the fusion devices. The erosion takes place by both physical and chemical sputtering due to impact of neutral particles and ions from the plasma with energies ranging from thermal energies to several keV. The eroded atoms can be redeposited in places close to the eroded area or they can be migrated through the scrape-off layer and deposited to distant areas. The underlying mechanisms of these phenomena require a good understanding in order to make predictions regarding the lifetime of wall components and to assess the amount of fuel retained in the machine. In 2010/11 the plasma-facing components (PFC) of the Joint European Torus (JET) were replaced by beryllium (Be) in the main chamber and tungsten (W) in the divertor, in order to exploit JET as a test bed for ITER since this material combination (Be and W) is foreseen for the activated phase of ITER [1, 2, 3]. Material migration and fuel retention were studied during the JET-ITER Like wall (ILW) experimental campaign 2011–2012 using in-situ techniques [4, 5] and post mortem analysis [6, 7, 8, 9, 10, 11, 12]. Widdowson et al. [13] give an overview of the material migration based on a detailed *in situ* photographic survey and post mortem analysis of passive diagnostics and selected tiles. Brezinsek et al. summarize in [14] the first conclusions from plasma-surface interaction processes in the Be/W material environment of the JET-ILW tokamak.

The current work refers to the surface analysis of samples retrieved from the JET-ILW tokamak divertor tiles after the first campaign. Specimens from four tiles of the divertor have been analyzed using ion-beam analysis (IBA), scanning electron microscopy (SEM) with energy dispersive X-ray (EDX) analysis, X-ray fluorescence spectroscopy (XRF) and X-ray diffraction (XRD). The aim of the paper is to provide a picture of the material erosion, deposition and migration using a comprehensive set of techniques in a number of selected tiles and thus to assist in the development of an overview and theoretical models of such phenomena. Notwithstanding that at ITER tungsten coated Carbon Fiber Composite (CFC) are not planned, results on W coatings are of major importance for JET-ILW and other machines (e.g. WEST) using the same or similar coating technology with tungsten.

2. Materials and Methods

Samples from the JET-ILW divertor Tiles 4, 6, 7 and 8 were analyzed (Table 1). The sample area varies between 1 and 2 cm^2 depending on the tile. The samples had been subjected to D-D plasma operation during the 2011-2012 campaign, which lasted for a total duration of 18.9 hours. These were carbon fiber composites (CFC) tiles coated with high-Z metal layers. The initial composition was as follows: CFC/Mo(3 µm)/W(12 µm)/Mo(4 µm)/W(4 µm) [15]. Mo is used as a buffer layer between the tungsten coating and the CFC substrate. In addition, a Molybdenum marker layer is deposited 4 µm below the tungsten top layer. In Table 1 the divertor tile number is given together with the so-called S-coordinate of each sample, which refers to its position, as shown in Fig. 1. S-coordinate denotes the poloidal distance along all divertor tiles.

Table 1. List and position of analyzed samples.

Sample Code	**Surface exposure to plasma**	**Divertor Tile number**	**S-coordinate**
14BN G**4**D/1a	Fully exposed	4	904
2BN G**6**C/2a	Poloidally in shadow of Tile 5	6	1360
2ON G**7**A/4a	Fully exposed	7	1699
2ON G**8**B/4a	Fully exposed	8	1892

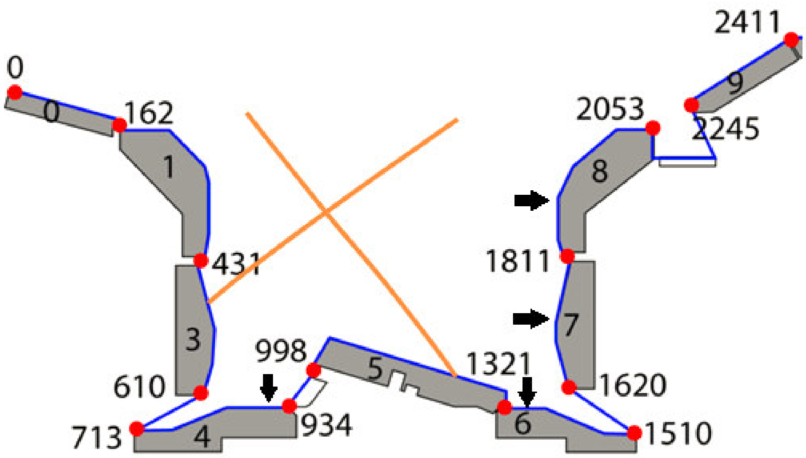

Fig. 1. Schematic drawing of the JET divertor poloidal cross section. Black arrows indicate the position of the analyzed samples

The samples were analyzed at the 5.5 MV Tandem Accelerator Laboratory of NCSR "Demokritos" (Athens, Greece) using the Nuclear Reaction Analysis (NRA) and Rutherford Backscattering (RBS) techniques employing a 1.7 MeV deuteron beam. The detection of the backscattered ions and nuclear reaction products (protons, deuterons and alphas) was performed using a silicon surface-barrier (SSB) detector placed at 170^o with respect to the beam axis. A thin (14 μm) Kapton foil was placed in front of the NRA detector to absorb the low-energy, elastically scattered deuterons, to avoid high pile-up background. Using this setup the beam current could go as high as 10 nA, thus enabling the faster and more accurate determination of the elements in the sample. Moreover, the proton peak coming from the $^{2}H(d,p)^{3}H$ reaction becomes visible due to the suppressed background. The whole setup was housed in a C. Evans & Assoc. scattering chamber equipped with a computer-controlled precision goniometer. The chamber was kept under vacuum (10^{-7} bar) with the aid of two turbo pumps.

The depth profile of beryllium, carbon, nitrogen and oxygen were determined, using the reactions $^{9}Be(d,p)^{10}Be$, $^{12}C(d,p)^{13}C$, $^{14}N(d,\alpha_1)^{12}C$ and $^{16}O(d,p)^{17}O$, respectively. The accumulated spectra were simulated with the aid of SIMNRA software package [16]. The differential cross sections used were derived by employing the SigmaCalc code by A. Gurbich and downloaded from the IBANDL database, IAEA [17]. The only exception was the case of the $^{9}Be(d,p)^{10}Be$ reaction where the dataset of I. I. Bondouk et al. [18] was used.

SEM measurements were carried out on a FEI Quanta Inspect scanning electron microscope (SEM) coupled with energy dispersive X-ray (EDX) spectroscopy. For the EDX analysis a voltage of 12.5 kV was used in order to enhance the contribution from the top layers of the samples (the calculated penetration depth is about 0.4 μm for tungsten).

The XRF spectra were measured employing Amptek's XRF system using a Ag X-ray tube, a high voltage of 30 kV and a silicon drift detector [19]. A collimator of 1 mm diameter was used. Elements with $Z>11$ are detected with a detection limit in the order of ppm. Spectrum analysis was performed using a NIST stainless steel 316 standard [20].

XRF and EDX analysis provide complementary information regarding the elemental concentration of the samples, with the XRF having higher sensitivity and ability to probe larger depths. Whereas XRF results refer to macroscopic areas of about 1 mm^2, EDX analysis has the advantage of yielding elemental concentration at microscopic scale.

XRD measurements were performed on a Bruker D8 spectrometer using Cu Kα radiation, a parallel beam stemming from a Göbbel mirror and VÄNTEC linear position-sensitive detector.

3. Results and Discussion

Two typical RBS/NRA spectra with and without the Kapton foil are presented in Figure 2. The use of the kapton foil results in the suppression of the high pile-up at low energies and allows for the appearance of the $^{2}H(d,p)^{3}H$ reaction peak. Moreover, in order to enhance the depth resolution, a higher amplification was used in the case of the detector with the Kapton foil keeping only the $^{14}N(d,\alpha_1)^{12}C$ peak within the spectrum limits. As this peak exhibits a higher cross section than the $^{14}N(d,\alpha_0)^{12}C$ and $^{14}N(d, p_0)^{15}N$ peaks it provides the lowest detection limits for nitrogen and it is the one used for the analysis. From the RBS/NRA measurements the atomic concentrations of D, Be, C, N, O and W were determined and are plotted in Fig. 3 as a function of depth for each of the four samples. It is noted that a flat surface is assumed in data analysis, which is not the case for the samples under investigation due to the roughness of the CFC substrates. It may be that the derived depth profiles do not reflect the exact layered structure of the sample. Nevertheless, the results for the deduced element stoichiometry are believed to be correct within 15%, taking into account all the experimental uncertainties. In Fig. 3 the top x-axis corresponds to the depth in the sample, which is calculated using the elemental concentration of each sublayer and its approximate mass density.

Most samples (Tiles 4, 7, 8) exhibit the same behavior regarding the depth profile of the light elements; the exception is the sample from Tile 6. Beryllium (Be), carbon (C) and deuterium (D) are detected in all samples. The wide peak of $^{12}C(d,p_0)^{13}C$ masks partly the peak $^{16}O(d,p_0)^{17}O$ and allows for only an approximate determination of the oxygen content in the samples from Tiles 4, 6 and 7, whereas in the sample from Tile 8 the oxygen content is below the detection limit. Beryllium originates from main wall transport through the plasma scrape-off layer (SOL) and co-deposition in the divertor region [21]. Carbon impurities are mainly related to the residual carbon from the previous wall from the tokamak components not replaced by the Be/W metallic ILW and, to some small extent, to the local damage of tungsten coating on CFC, from the exposure of the substrate to plasma. The latter is confirmed from micro proton-induced X-ray emission (PIXE) mapping measurements (not presented here) which show the lack of tungsten in very small areas of the divertor tiles investigated. Nitrogen (N) is detected only in Tile 6 due to its high concentration; its content in the samples from the other Tiles is below the detection limit. It is noted that in the previous study of the same samples, employing ion-beam analysis, without the use of a Kapton filter between the sample and the detector, Nitrogen could be quantified in all Tiles [22] most probably due to the accumulation of a higher beam charge. Nitrogen presence in the divertor Tiles is due to the plasma edge cooling using nitrogen gas and this is co-deposited with other materials on the plasma wall components. The same effect has been found in other studies [9]. Oxygen exists in the tiles prior to plasma exposure; it is also due to oxygen gettering of the surfaces of Be Tiles of the main tokamak chamber, as well as the oxidation of all components when exposed to air.

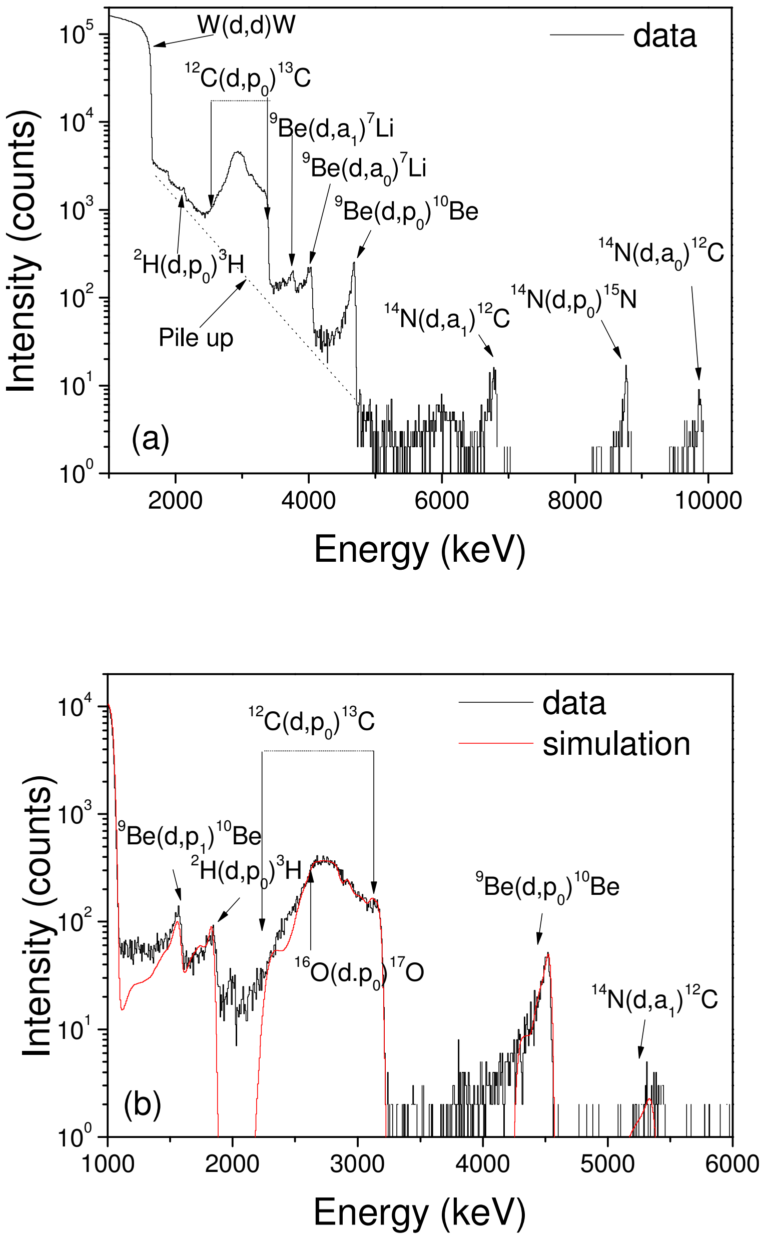

Fig. 2. RBS/NRA spectrum of 2BN G6C/2a sample (a) without kapton foil and (b) with kapton foil. The red line in (b) is the simulated curve.

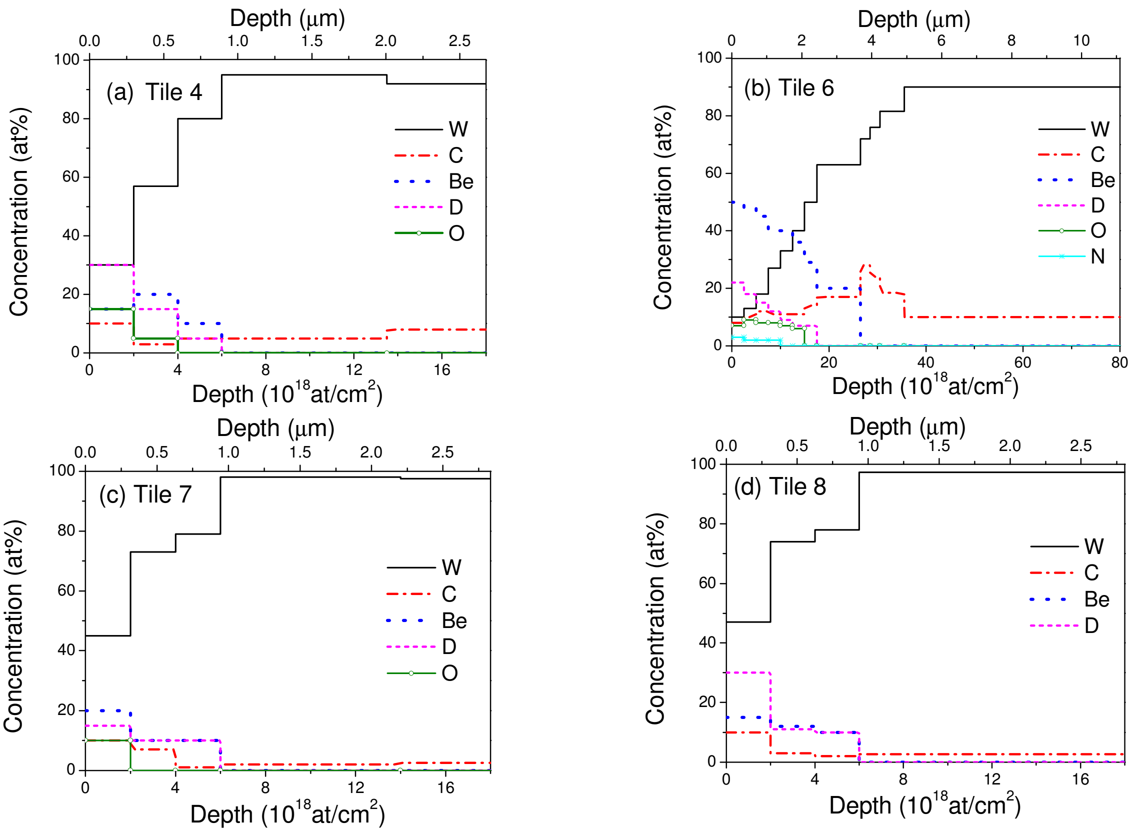

Fig. 3. Atomic concentrations for samples (a) 14BN G4D/1a, (b) 2BN G6C/2a and (c) 2ON G7A/4a, (d) 2ON G8B/4a.

The overall thickness of the light elements deposition on the samples from Tiles 4, 7 and 8, except for C, is around 6 x 10^{18} at/cm^2, whereas for Tile 6 it is slightly above 25 x 10^{18} at/cm^2. The depth profile of Be does not exceed the depth of 5 x 10^{18} at/cm^2 with the sole exception of 2BN G6C/2a (Tile 6) sample, for which Be reaches depths of about 25 x 10^{18} at/cm^2. Regarding the presence of C in these samples, it seems that it extends to depths greater than 18 x 10^{18} at/cm^2 for Tiles 4, 7 and 8 with a very slow decreasing profile, except for the sample from Tile 6 where C is traced at 80 x 10^{18} at/cm^2 with an almost constant profile. The fact that deuterium's concentration reaches its highest value for Tile 6, which presents the thickest deposit, is in agreement with the findings of Heinola et al. [10], where it is reported that the highest figures for fuel retention are obtained from regions with the thickest deposited layers. The fact that Tile 6 presents the thickest deposit must be related to its adjacent position with the outer strike point (see Fig.1). The Be film thickness obtained by Ruset et al. using glow discharge optical emission spectrometry [23] is in agreement with the values obtained in the current study.

In order to be able to compare the current results with those of ion-beam analysis from samples on adjacent positions in the JET tokamak divertor [8, 9, 24], the surface concentrations (up to a depth of around 0.8 μm for the samples from Tiles 4, 7 and 8 and up to 4 μm for Tile 6) are given in Table 2 together with the light elements-to-Be ratio, down to the depth the light element is present. The total amount of C found in Tiles 4, 7 and 8 is in agreement with that found in [9]. However, this is not the case for Tile 6; in the current study a higher, by an order of magnitude, amount of C is found and this is in agreement with the results of Mayer et al. [24]. The surface concentrations of O are comparable with those found in [9]. The total amount of Be found in all samples is in good agreement with that obtained by Heinola et al. [10] and Mayer et al. [24]. Furthermore, Baron-Wiechek et al. [8] found that the maximum Be concentration in Tiles 3, 4, 6 and 7 is less than 1×10^{18} at/cm^2 which is in general agreement with the findings of the current study for Tiles 4 and 7, but there is a considerable discrepancy for Tile 6 for which a value of 9×10^{18} at/cm^2 is obtained (Table 2). However, the same authors report that higher than 2.5×10^{18} at/cm^2 deposition of Be is found on the sloping region of Tile 6, which is close to the S-coordinate of the sample from Tile 6 under investigation. For N the numbers in parenthesis in Table 2 correspond to the expected atomic surface density employing the corresponding results obtained without the use of a Kapton foil [22]. It is pointed out that the values obtained for the N atomic surface density for the sample from Tile 6, with and without the use of the Kapton foil, are in very good agreement with each other.

Table 2. The integrated atomic surface density of light elements (top). Light elements ratio with respect to Be (bottom). For the numbers in parenthesis see text.

	Atomic surface density (10^{18} at/cm^2)			
element	Tile 4	Tile 6	Tile 7	Tile 8
C	0.36	3.46	0.36	0.30
Be	0.90	9.00	0.80	0.74
D	1.0	2.25	0.70	1.02
O	0.40	1.13	0.20	0
N	0 (0.023)	0.23	0 (0.092)	0 (0.058)

	Tile 4	Tile 6	Tile 7	Tile 8
C/Be	0.4	0.38	0.45	0.41
O/Be	0.44	0.125	0.25	0
N/Be	0 (0.026)	0.025	0 (0.12)	0 (0.078)

The XRF measurements show the presence of Cr, Fe, Ni, Mo and W. Fe, Cr and Ni are transported from the steel or Inconel alloy components in the main tokamak chamber. Mo originates from both the marker layer in tungsten coated divertor Tiles, the erosion of Inconel 625 parts of the radio frequency antenna [9] and probably the erosion of Tile 3 which has Mo as a plasma facing coating [10]. It is noted that although the main part of the XRF spectrum from Mo comes from the marker layer the obtained atomic concentration of Mo is less than that of W because of the absorption of the outcoming X-ray beam by the W layer on top of the Mo one. The concentration (in at%) found for elements with $Z>11$ is given in Table 3. The stoichiometry should be viewed only as relative. Although the Ni peak was detected in all samples, Ni could be quantified only for the sample from Tile 6. This happens because the Ni K_{α} peak (7.48 keV) overlaps with the L_{β} peak (7.39 keV) from W. The sample from Tile 6 has the highest concentration of the Inconel elements Cr, Fe and Ni. High Fe concentration is also found for the sample from Tile 7.

Table 3. Elemental concentration in at% obtained from XRF measurements. The numbers in parenthesis are the standard deviations.

	Concentration (at%)			
	14 BN G4D/1a	**2BN G6C/2a**	**2ON G7A/4a**	**2ON G8B/4a**
Cr	0.053(9)	0.602(3)	0.07(1)	0.14(2)
Fe	0.035(6)	0.4(2)	0.543(8)	0.12(1)
Ni	n.q.*	2.324(3)	n.q.	n.q.
Mo	23.07(7)	23.49(5)	24.59(8)	26.98(7)
W	76.84(7)	73.17(5)	74.79(8)	72.76 7)

* n.q. stands for non-quantifiable

SEM measurements on the surface of the samples show the characteristic cauliflower structure, as it is depicted in Fig. 4 for the sample from Tile 7 (2ON G7A/4a) in secondary electrons and in backscattered electrons (BSE) mode. In the BSE image the light elements are appearing darker and heavy elements are appearing brighter. The roughness observed is due to the CFC substrate. A similar surface morphology is observed for the samples from Tiles 4 and 8 (not shown). The sample from Tile 6 presents a rather different morphology, as it is presented in Fig. 5, with enhanced material deposition compared to the other samples, with enhanced light element deposition in the valleys of the rough surface. This may be due to erosion of Tile 6 and material re-deposition or material deposition from the erosion of the adjacent Tile 5.

EDX analysis was performed on different regions with light gray and dark color in backscattered electron mode. The deduced elemental concentrations are presented in Table 4. It is noted that, in general, EDX analysis has less sensitivity than XRF spectroscopy and probes smaller depths than XRF.

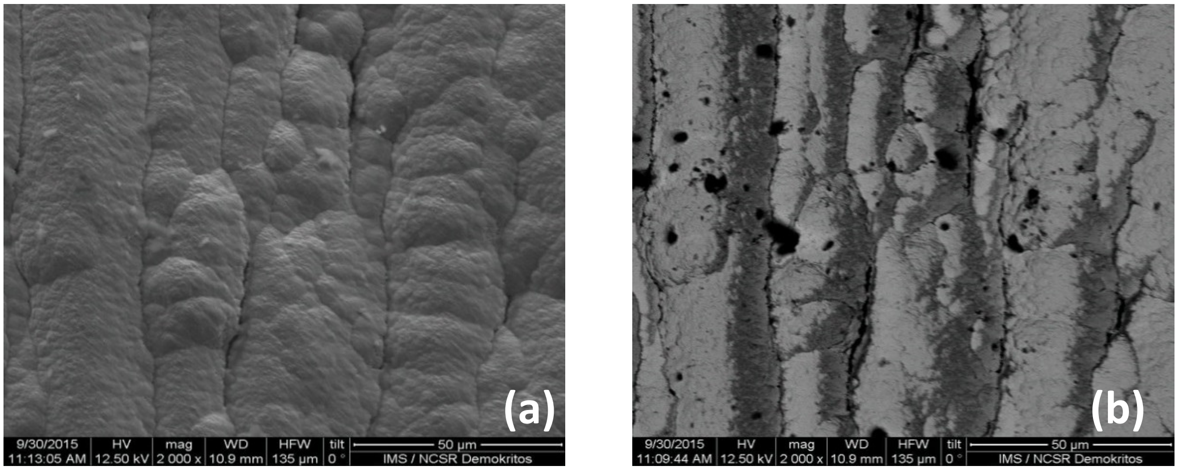

Fig. 4. SEM images of the surfaces of the sample 2ON G7A/4a in (a) secondary electrons mode and in (b) backscattered electrons.

Images in Fig. 4 show surface features of the W coating with thin co-deposits on Tile 7. From the secondary electron image in Fig. 4a one may infer that no damage to the coating has occurred. The black spots observed in Fig. 4b in backscattered mode are carbon-rich areas with the C concentration in the range of 90-93.5 at%. It is most probably related to the non-deposition of light impurities in the “valleys” which form local shadowed micro-areas, as discussed earlier [25, 26]. The dark areas in the sample from Tile 6 (Fig. 5b) are rich in C, N, Cr, Fe, Ni and Mo, thus confirming the role of surface roughness in the accumulation of co-deposited species [27]. Since the probing depth of EDX in tungsten is around 0.4 µm, the detection of Mo indicates that this Mo does not originate from the marker layer, but from the erosion of the Inconel 625 parts in the main chamber, as mentioned previously. Nitrogen is found only in Tile 6, which is in agreement with the RBS/NRA results shown in Table 2, taking into account the much smaller sensitivity of the method in elemental detection. Also the Ni:Fe:Cr ratio found with XRF for Tile 6 coincides with that found by EDX analysis. The enhanced W content in Tile 6, compared to the samples from the other tiles, is in agreement with the finding of Mayer et al. [24] that in Tile 6 the tungsten thickness is increased by around 500 nm due to erosion from the adjacent Tile 5 (outer strike point, see fig. 1) and re-deposition on Tile 6.

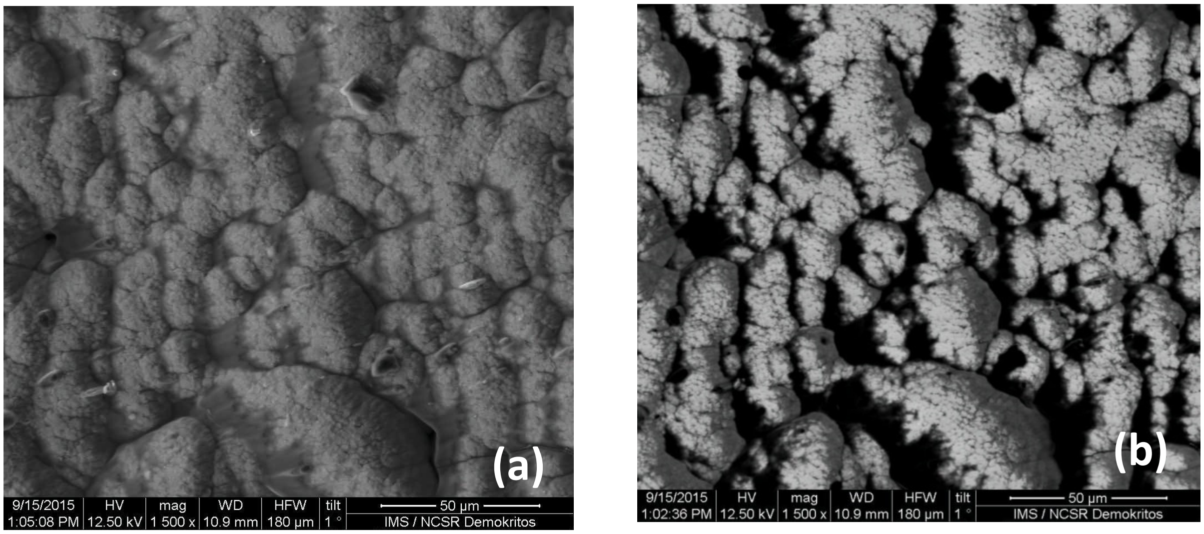

Fig. 5. SEM images of the surfaces of the sample 2BN G6C/2a in (a) secondary electrons mode and in (b) backscattered electrons.

Table 4. Elemental concentration in at% derived from EDX measurements.

	Concentration (at%)							
	14 BN G4D/1a		**2BN G6C/2a**		**2ON G7A/4a**		**2ON G8B/4a**	
	Gray area	Dark area	Gray area	Dark area	Gray area	Dark area	Gray area	Dark area
C	32.4-33.5	92.9-93.5	18.5	30.6-35.0	22.3-26.2	90.0-93.8	17.8	95.4
N	-	-	-	10.3-12.9	-	-	-	-
O	10.5-15	2.5-3.4	10.1	17.3-17.9	3.4-4	1.5-1.9	2.2	1.8
Cr	-	-	-	2.1-2.5	-	-	-	-
Fe	-	-	-	1.9-2.4	-	-	-	-
Ni	-	-	1.6	11.5-12.3	-	-	-	-
Mo	0.7-0.9	-	-	0.6	-	-	-	-
W	50.8-56.2	3.8-4.0	69.8	18.7-23.5	69.9-74.3	4.7-8.1	80.0	2.8

XRD measurements were performed on all samples to investigate the possible formation of any compound during co-deposition of materials. The XRD spectra are shown in Fig. 6 in logarithmic scale and are displaced in y-axis for clarity. From the code names of the samples only the part that indicates the Tile number is given. Bragg peaks of W and Mo are clearly observed in all the samples. The transport of Be from the main chamber to the divertor is also confirmed by the XRD measurements; the strongest (101) Bragg peak of hexagonal α-Be (Space Group P63/mmc) is found mainly in the samples from Tiles 7 and 8. Although the RBS/NRA results show that the sample from Tile 6 has the highest Be content, this discrepancy with the XRD results may be due to the fact that XRD beam “sees” a much larger portion of the sample of around 10 mm^2, whereas in RBS/NRA measurements the diameter of the beam is 1 mm, and the result may not be representative of the whole sample. Also C with Space Group R-3m, which may be due to carbon transport from the main tokamak chamber, is detected in the samples from Tiles 4 and 6. Furthermore, the XRD spectra indicate the formation of W_2C compound in all the samples with the more intense Bragg peak in the samples from Tiles 6 and 7. The tungsten carbide is likely to be formed from the carbon being transferred from the tokamak main chamber to the divertor. It is noted that XRD measurements carried out on tungsten coated CFC samples not exposed to plasma showed no indication of tungsten carbide formation. Such a layer, if it is continuous and it is formed at the top surface, is expected to act as a protective coating against the formation of W-Be compounds. The formation of compounds such as W-Be, BeO or W-N could not be identified. Possible formation of tungsten nitride is expected to be advantageous since its presence reduces the tungsten erosion, and furthermore it has extreme hardness, good chemical resistance, high electrical conductivity and high melting point [28].

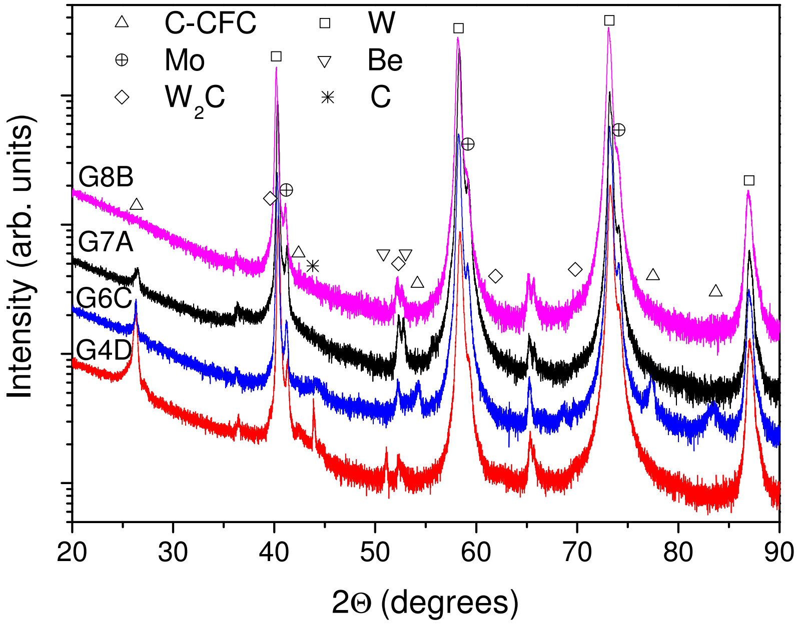

Fig. 6. XRD spectra in logarithmic scale showing the detected phases. The spectra are displaced in y-axis for clarity.

4. Conclusions

Studies performed with a comprehensive set of methods on samples retrieved after 18.9 h of plasma operation from the JET-ILW divertor have revealed several important facts regarding the structure and composition of surfaces. It should be stressed that for the first time in studies of materials from JET a deuterium beam has been used to trace in low-Z species (D, Be, C, N, O) with particular emphasis on the quantification of nitrogen. It is known that nitrogen is retained in PFC [9], but those previous studies were limited to the outermost layer of the sample surface. Substantial amounts quantities of nitrogen have been detected on the specimen from Tile 6, i.e. divertor bottom in the area shadowed poloidally by bulk tungsten Tile 5. The samples from Tiles 4, 7 and 8 exhibit very similar deposition patterns as a function of depth with the light elements (C, O, D and Be) extending to a depth of around 1 µm. The situation is different for the sample taken from Tile 6 where the concentration of the light elements is not only higher compared to the samples from the other tiles but they also reach larger depths of about 4 µm. Fuel retention is higher in Tile 6 but of the same order of magnitude in all tiles studied. Moreover, Fe, Ni, Cr and Mo are also deposited on the divertor tiles due to the erosion of the Inconel 625 parts in the main chamber. Also XRD measurements were performed for the first time. The results clearly show that surfaces are virtually free from compounds, especially low melting point Be-W intermetallics, which could drastically change thermo-mechanical properties and surfaces and then have an impact on the power handling and the integrity of the components. The presence of the tungsten carbide (W_2C) has been detected, but this phase is only a minor component in the diffractogram. This study will be extended to materials retrieved from JET after longer operation periods covering three ILW campaigns.

Acknowledgments

This work was carried out within the EUROfusion Consortium and received funding from the EURATOM research and training programme 2014-2018 under grant agreement number No 633053. The views and opinions expressed herein do not necessarily reflect those of the European Commission.

References

[1] Matthews G.F. *et al* 2011. Jet ITER-like wall – overview and experimental programme *Phys. Scr.* **T145** 014001

[2] Matthews G.F. *et al* 2014 The second phase of JET operation with the ITER-like wall Phys. Scr. T159 014015

[3] Rubel M. *et al* 2013. Overview of erosion-deposition diagnostic tools for the ITER-Like Wall in the JET tokamak *J. Nucl. Mater.* **438** S1204

[4] Brezinsek S. *et al* 2013. Fuel retention studies with the ITER-Like Wall in JET *Nucl. Fusion* **53** 083023

[5] Brezinsek S. *et al* 2013. Residual carbon content in the initial ITER-Like Wall experiments at JET *J. Nucl. Mater.* **438** S303

[6] Coad J. P. *et al* 2014. Surface analysis of tiles and samples exposed to the first JET campaigns with the ITER-like wall *Phys. Scr.* **T159** 014012

[7] Heinola K., Ayres C.F., Baron-Wiechec A., Coad J.P., Likonen J., Matthews G.F., Widdowson A. and JET-EFDA Contributors 2014. Tile profiling analysis of samples from the JET ITER-like wall and carbon wall *Phys. Scr.* **T159** 014013

[8] Baron-Wiechec A. *et al* 2015. Global erosion and deposition patterns in JET with the ITER-like wall *J. Nucl. Mater.* **463** 157

[9] Petersson P., Rubel M., Esser H.G., Likonen J., Koivuranta S., Widdowson A. and JET-EFDA Contributors 2015. Co-deposited layers in the divertor region of JET-ILW *J. Nucl. Mater.* **463** 814

[10] Heinola K. *et al* 2015. Fuel retention in JET ITER-Like Wall from post-mortem analysis *J. Nucl. Mater.* **463** 961

[11] Hatano Y., Widdowson A., Bekris N., Ayres C., Baron-Wiechec A., Likonen J., Koinuranta S., Likonen J., Yumizuru K. and JET EFDA Contributors 2015. 2D tritium distribution on tungsten tiles used in JET ITER-like wall project *J. Nucl. Mater.* **463** 966

[12] Hatano Y., Yumizuru K., Likonen J., Koivuranta S., Likonen J. and JET Contributors 2016. Tritium distributions on tungsten and carbon tiles used in the JET divertor *Phys. Scr.* **T167** 014009

[13] Widdowson A. et al. 2014. Material migration patterns and overview of first surface analysis of the JET ITER-like wall *Phys. Scr.* **T159** 014010

[14] Brezinsek S. and JET-EFDA Contributors 2015. Plasma-surface interaction in the B e/W environment: Conclusions drawn from the JET-ILW for ITER *J. Nucl. Mater.* **463** 11

[15] Ruset C., Grigore E., Maier H., Neu R., Li X., Dong H., Mitteau R., Courtois X. and JET EFDA Contributors 2007. Tungsten coatings deposited on CFC tiles by the combined magnetron sputtering and ion implantation technique *Phys. Scr.* **T128** 171

[15] Mayer M. 1999. SIMNRA, a Simulation Program for the Analysis of NRA, RBS and ERDA AIP Conf. Proc. **475** 541

[17] http://www-nds.iaea.org/ibandl/

[18] Bondouk I.I., Asfour F. and Machali F. 1974. An experimental investigation of the Reactions ^{9}Be(d,p$_0$)^{10}Be and ^{9}Be(d,p$_1$)^{10}Be in the Energy Range 0.9-2.5 MeV *Rev. Roum. Phys.* Vol. 19 1053

[19] http://amptek.com/product/complete-xrf-experimenters-kit/

[20] NIST SRM 160b, https://www-s.nist.gov/srmors/view_cert.cfm?srm=160B

[21] Loarer T. *et al* 2013. Comparison of long term fuel retention in JET between carbon and the ITER-Like Wall *J. Nucl. Mater.* **438** S108

[22] Tsavalas *et al* 2016. Investigation of the ITER-like wall divertor Tiles at JET tokamak *25th HNPS Symposium*, Athens, 3 – 4 June 2016 (in press)

[23] Ruset C., Grigore E., Luculescu C., Tiseanu I., Likonen J., Mayer M., Rubel M., Mattews G.F. and JET Contributors 2016. Investigation on the erosion/deposition processes in the ITER-like wall divertor at JET using glow discharge optical emission spectrometry technique Phys. Scr. **T167** 014049.

[24] Mayer et al. 2016. Erosion and deposition in the JET divertor during the first ILW campaign *Phys. Scr.* **T167** 014051

[25] Petersson P., Rubel M., Possnert G. and Pegourie B. 2011. Micro-distribution of fuel and metal in carbon-based plasma-facing materials *Phys. Scr.* **T145** 014014

[26] Bykov I., Bresgsaker, H., Petersson P., Likonen j. and Possnert G. 2014. Quantitative plasma-fuel and impurity profiling in thick plasma-deposited layers by means of micro ion beam analysis and SIMS *Nucl. Instr. Meth.* **B332** 280

[27] Rubel M., Fortuna E., Kreter A., Wessel E., Philipps V. and Kurzyblowski K.J. 2006. Overview of comprehensive characterisation of erosion zones on plasma facing components *Fusion Eng. Des.* **81** 211

[28] Alegre D., Acsente T., Martin-Rojo A. B., Oyarzabal E., Tabarés F. L., Dinescu G., De Temmerman G., Birjega R., Logofatu C., Kovac J., Mozetic M. 2015. Characterisation of tungsten nitride layers and their erosion under plasma exposure in NANO-PSI *Romanian Reports in Physics*, **67**, 532